

ATP-dependent mechanics of red blood cells

Timo Betz¹, Martin Lenz, Jean-François Joanny, and Cécile Sykes

Centre de Recherche, Institut Curie, Unités Mixte de Recherche 168, F-75248 Paris, France

Edited by Thomas D. Pollard, Yale University, New Haven, CT, and approved July 20, 2009 (received for review April 28, 2009)

Red blood cells are amazingly deformable structures able to recover their initial shape even after large deformations as when passing through tight blood capillaries. The reason for this exceptional property is found in the composition of the membrane and the membrane-cytoskeleton interaction. We investigate the mechanics and the dynamics of RBCs by a unique noninvasive technique, using weak optical tweezers to measure membrane fluctuation amplitudes with μs temporal and sub nm spatial resolution. This enhanced edge detection method allows to span over >4 orders of magnitude in frequency. Hence, we can simultaneously measure red blood cell membrane mechanical properties such as bending modulus $\kappa = 2.8 \pm 0.3 \times 10^{-19}\text{J} = 67.6 \pm 7.2 k_B T$, tension $\sigma = 6.5 \pm 2.1 \times 10^{-7}\text{N/m}$, and an effective viscosity $\eta_{\text{eff}} = 81 \pm 3.7 \times 10^{-3}\text{Pa s}$ that suggests unknown dissipative processes. We furthermore show that cell mechanics highly depends on the membrane-spectrin interaction mediated by the phosphorylation of the interconnection protein 4.1R. Inhibition and activation of this phosphorylation significantly affects tension and effective viscosity. Our results show that on short time scales (slower than 100 ms) the membrane fluctuates as in thermodynamic equilibrium. At time scales longer than 100 ms, the equilibrium description breaks down and fluctuation amplitudes are higher by 40% than predicted by the membrane equilibrium theory. Possible explanations for this discrepancy are influences of the spectrin that is not included in the membrane theory or nonequilibrium fluctuations that can be accounted for by defining a nonthermal effective energy of up to $E_{\text{eff}} = 1.4 \pm 0.1 k_B T$, that corresponds to an actively increased effective temperature.

erythrocyte | membrane fluctuations | nonequilibrium | optical tweezer | spectrin

The extraordinary deformability of RBCs is vital for their proper function, as it enables the cells to be elongated by more than twice their size when passing through μm -sized capillaries. The elastic properties of RBCs are dominated by the interaction between the cell membrane and the underlying cytoskeleton, mainly consisting of spectrin, a long heterodimer that aligns tail to tail forming a 200-nm-long tetramer. Each spectrin filament interconnects to up to 5 other spectrins and is bound to the cell membrane via a protein complex consisting of protein 4.1R, actin, and glycophorin C (1). The plasma membrane fluctuations are related to RBCs' mechanical properties that have been extensively studied over the past three decades (2–6). It is well known that fluctuations of the membrane depend on its bending rigidity κ and its membrane tension σ (7). Furthermore, RBCs gain their elasticity from the elastic shear modulus of the cytoskeletal spectrin network (8, 9). Recent theoretical analysis (10) suggest that the spectrin cytoskeleton acts as a steric barrier restricting membrane undulations toward the network.

Experiments by Tuvia and coworkers showed an ATP dependent effect by monitoring the static fluctuation amplitude of RBCs under normal and ATP-depletion conditions (11). In these measurements, the fluctuation amplitude (the root mean square displacement; *rmsd*), was found to decrease substantially under ATP depletion. This was interpreted as a sign for activity-dependent fluctuations. However, a recent report did not confirm this decrease (6), arguing that the fluctuations are purely

thermally driven. Additionally to the fluctuation decrease under ATP depletion, Tuvia et al. found a fluctuation decrease upon increase of the external medium viscosity, in disagreement with thermodynamics, which predicts that all equilibrium quantities are independent of transport coefficients such as the viscosity. This suggested an active, energy-consuming process, depending on phosphorylation of the 4.1R protein or erythrocyte myosin motors. Subsequent theoretical studies argue that the viscosity dependence of static fluctuations could be explained by the ATP-dependent phosphorylation of the 4.1R protein (12), which controls the spectrin-membrane connection (1). This phosphorylation is catalyzed by protein kinase C (PKC) (13), which disassembles the 4.1R/spectrin/actin trimer, thus leading to a decreased overall stability of the RBC membrane.

Previous measurements to determine membrane fluctuations suffer from the restricted time resolution of camera acquisition (6), or can only detect relative and uncalibrated fluctuation amplitudes (5, 11). To overcome both limitations we used a unique approach to monitor the time-dependent fluctuation of the RBC membrane at a single point with sub nm spatial and μs time resolution (14). Our measurements are in excellent agreement with the theory of fluctuating membranes at frequencies $>10\text{Hz}$ and enable us to simultaneously measure the membrane bending modulus κ , the tension σ , and an effective viscosity η_{eff} of RBCs, thereby showing that the external viscosity has no effect on the time averaged fluctuation amplitudes.

Results

Interferometric Fluctuation Detection. The method used to measure RBC membrane fluctuations is an extension of well-known interferometric particle detection using optical tweezers (15). However, the laser is operated at minuscule powers ($\approx 50\ \mu\text{W}$) at the sample, too small to create a trapping potential. In the experiments, a volume of 15 μL of a RBC suspension was sealed between two coverslips, and cells were allowed to weakly attach on the substrate for 30 min. Only discocyte-shaped RBCs with diameters varying from 6 to 8 μm were used. Weak attachment of the RBCs to the coverslip was checked by reflection interference contrast microscopy (RICM) (*SI Appendix* and *Fig. S1*). The infra-red ($\lambda = 1064\text{ nm}$) laser was positioned at the edge of the cell, and a calibration curve (line scan) was acquired by moving the RBC through the laser with a step size of 4 nm using a piezoelectric stage and recording the signal with a quadrant photodiode (QPD) at the condenser's back focal plane as shown in *Fig. 1*. The method is based on a difference in refractive index, thus detecting the plasma membrane at the interface between the cell and the medium. Each data point of the calibration curve represents an average of 500 recordings taken at a sampling rate of 100 kHz. The acquired calibration curve shows a linear regime, which was used to convert between QPD voltage and edge position in nm by determining the slope. To record the fluctuations, the edge of the RBC was positioned at the

Author contributions: T.B. and C.S. designed research; T.B. performed research; T.B., M.L., and J.-F.J. analyzed data; and T.B. and C.S. wrote the paper.

The authors declare no conflict of interest.

This article is a PNAS Direct Submission.

¹To whom correspondence should be addressed. E-mail: timo.betz@curie.fr.

This article contains supporting information online at www.pnas.org/cgi/content/full/0904614106/DCSupplemental.

Table 1. Collection of mechanical parameters of RBCs under various conditions, compared with previous findings by Evans et al. (6) and Strey et al. (4)

| | Normal | ATP-depl. | PKC |
|---------------------------------------|----------------|----------------|----------------|
| $rmsd_{ex}$ [nm] | 33.0 ± 1.3 | 22.3 ± 0.6 | 36.7 ± 2.8 |
| $rmsd_{th}$ [nm] | 36.3 ± 12 | 24.0 ± 9.0 | 47.2 ± 13 |
| κ_{SPS}^{stat} [10^{-19} J] | 2.8 ± 0.2 | 6.1 ± 0.3 | 2.3 ± 0.4 |
| κ^{dyn} [10^{-19} J] | 2.8 ± 0.3 | 3.9 ± 0.3 | 2.6 ± 0.2 |
| σ [10^{-7} N/m] | 6.5 ± 2.1 | 19 ± 1 | 2.7 ± 1.1 |
| η_{eff} [10^{-3} Pa s] | 81 ± 3.7 | 118 ± 11.8 | 57 ± 2.4 |
| $rmsd_{Evans}$ [nm] | 23.6 ± 0.6 | 22.8 ± 1.0 | — |
| $rmsd_{Strey}$ [nm] | 30.0 ± 5 | — | — |

$rmsd_{th} = 36 \pm 11$ nm, which is calculated using the mechanical parameters determined from the dynamic measurements (Table 1). Additionally, in the literature the $rmsd$ has been used to determine the bending stiffness by assuming a tensionless limit and accounting for the shear modulus on the first fluctuation mode. Strey, Peterson, and Sackmann (SPS) established an approximation to calculate a bending modulus from the $rmsd$ (4): $\kappa_{SPS}^{stat} = (6 \times 10^{-6})k_B T R^2 / (\Delta h_l = 1)^2 = 2.8 \pm 0.2 \times 10^{-19}$ J, where R denotes the cell radius, and k_B the Boltzmann constant. This approximative static bending modulus is an alternative method, and in the case of normal RBCs it agrees well with the dynamic bending modulus obtained from the PSD (see Table 1). We furthermore checked the dependence of the fluctuation on the viscosity of the external medium. We increased the medium viscosity by the addition of 75 mg/mL ($\eta_{75} = 2.4 \pm 0.1 \times 10^{-3}$ Pa s), 135 mg/mL ($\eta_{135} = 4.4 \pm 0.2 \times 10^{-3}$ Pa s), and 200 mg/mL ($\eta_{200} = 10.9 \pm 0.9 \times 10^{-3}$ Pa s) of Dextran 41000. In all cases fluctuation histograms were well Gaussian distributed, but did not depend on the external viscosity (Fig. 2B), as expected from equilibrium statistical mechanics. Furthermore, we used the PSD of RBC immersed in solvents of different viscosities to determine the effective viscosity as a function of external viscosity. The resulting dependence (SI Appendix and Fig. S3) can be well fitted with a linear function $\eta_{eff} = a \times \eta_{ext} + b$, yielding fit parameters of $a = 8.3 \pm 2.3$ and $b = 53 \pm 11 \times 10^{-3}$ Pa s.

PSD of ATP-Depleted Cells. To investigate the effect of ATP on membrane mechanics, we removed ATP from the RBCs by applying an ATP depletion medium for 3 h and then measured the resulting PSD. As presented in Fig. 3A (green, $n = 200$, fit quality: $r^2 = 0.85$) the fluctuation amplitude was significantly smaller than for the normal RBCs over the full frequency spectrum, showing a strong dependence of the membrane fluctuations on ATP. We measured a slightly increased bending rigidity, and dynamic measurements showed that the effective viscosity was also increased by $\approx 50\%$ (Table 1). The effect of ATP-depletion was additionally reflected in the static measurement of the $rmsd$, which was strongly decreased compared with normal cells (Table 1). Interestingly, removing ATP led to a strong increase of tension, which explains the discrepancy between the dynamic bending modulus presented in this work and the static bending modulus which assumes a vanishing tension (4) (Table 1).

PSD of PKC-Activated Cells. The fluctuation decrease in ATP-depleted cells might be because of an inhibition of the phosphorylation of the 4.1R protein, which connects the spectrin to the membrane in its unphosphorylated state (13). To investigate the influence of this connection we activated PKC, an enzyme that had been shown to phosphorylate 4.1R, thus resulting in an increased dissociation of the spectrin network and unbinding of spectrin from the membrane (13). The resulting PSD of 21 PKC activated cells is

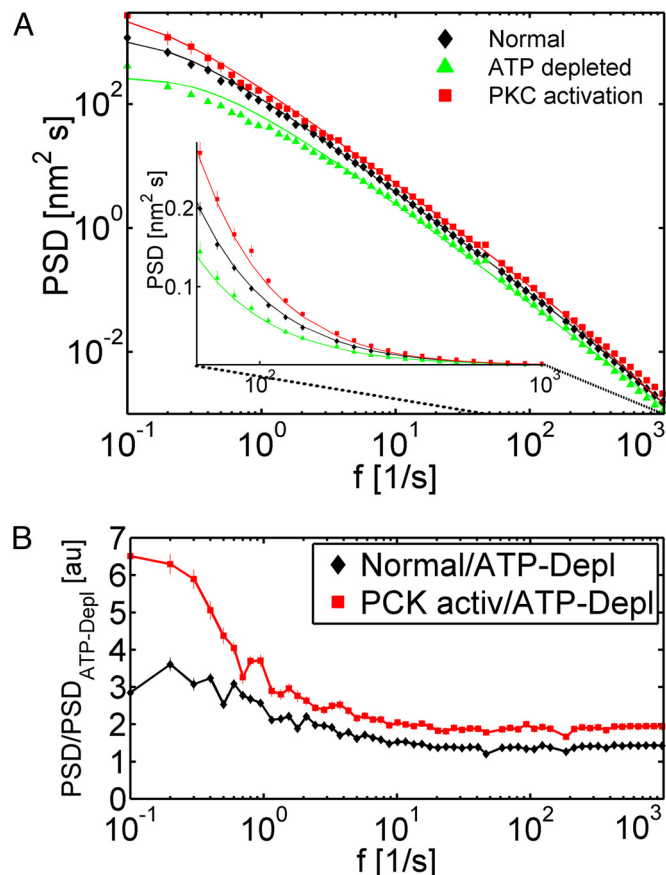


Fig. 3. Absolute and normalized fluctuation spectra. (A) Mean PSD of 21 normal RBCs ($n = 210$, black) and 20 ATP-depleted ($n = 200$, green) and 21 PKC-activated ($n = 210$, red). The solid lines show the fit. (Inset) Semilog plot of the same data for the marked frequency range showing that the ATP-depleted cells have the smallest amplitude. (B) Semi logarithmic representation of the fluctuation amplitudes normalized by the ATP-depleted PSD, which can be considered to be a purely thermally driven system because of the lack of the energy source ATP.

presented in Fig. 3A (red, $n = 210$, fit quality: $r^2 = 0.97$). Fluctuations increased over the accessible frequency range compared with the normal RBCs. The analysis of the data yields static and dynamic bending rigidities consistent with the bending rigidity measured on normal RBCs (Table 1). However, our results showed that over-activation of PKC decreases membrane tension by $\approx 50\%$ and resulted in a slight decrease of the effective viscosity (Table 1). DMSO control experiments showed no difference with the normal cells. Additionally, we checked the effect of cells treated with the actin depolymerizing drug latrunculin A (SI Appendix and Fig. S4). The data are similar to the PKC activated cells (SI Appendix and Fig. S5), however, our controls show that F-actin in RBCs was not affected by latrunculin A (SI Appendix and Fig. S6), which indicates that there is no actin dynamics in RBCs. Our experiments suggest a yet unknown effect of LA on the cytoskeleton membrane interaction.

Relative Fluctuation Amplitudes. To investigate the effect of non-thermal contributions, we normalized the fluctuations of normal and PKC-activated cells by the PSD of ATP-depleted cells (Fig. 3B). A striking result of this normalization arose at frequencies >10 Hz, where all relative amplitudes level off to plateaus. Here, the fluctuations for PKC-activated cells level to a value of approximately twice the fluctuation of ATP-depleted cells, and the amplitude of normal cells was $\approx 30\%$ higher than in ATP-

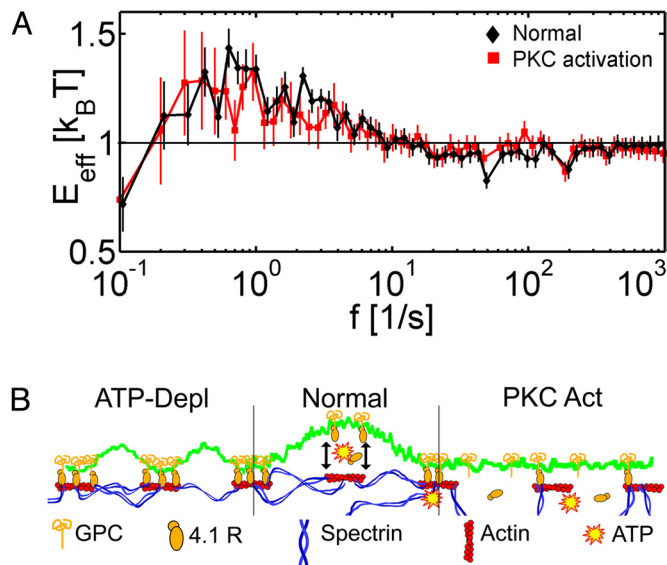


Fig. 4. Effective energy and membrane model. (A) Frequency-dependent energy for the various cells. At high frequencies, the fluctuations are driven by thermal activation shown by the value of $1 k_B T$, whereas for low frequencies the maximal effective energy is, $E_N^{max} = 1.43 \pm 0.09 k_B T$ for normal cells and $E_P^{max} = 1.32 \pm 0.08 k_B T$ for the PKC-activated cells. (B) Model to explain the measured mechanical differences (17). The fluctuations depend on the membrane properties and on the integrity of the underlying spectrin cytoskeleton, connected to the membrane by actin, glycoprotein C (GPC), and protein 4.1R. In normal cells, a continuous de- and reattachment of the spectrin results in a certain net tension. ATP depletion increases the spectrin-membrane connection and the integrity of the spectrin network, leading to an increased tension. In contrast, disrupting the spectrin-membrane interaction by PKC activation weakens the spectrin network and hence decreases the measured tension.

one for the high frequency domain ($f > 10\text{Hz}$) in all RBC conditions. Hence, in this regime the passive equilibrium membrane theory seems to be a correct description. However, we observe for the low frequency part a deviation from one, leaving up to 40% of the fluctuations unaccounted for (Fig. 4A). This discrepancy can be potentially explained in two ways. First, at low frequency the simple membrane description of the complex RBC membrane yielding the function g might break down. Hence, it would be necessary to extend the model, for example to composite membrane systems explicitly including the spectrin. A second possible explanation is the breakdown of the equilibrium description, leading to a frequency-dependent effective energy $E_{eff}(f)$ that becomes important at frequencies $< 10\text{Hz}$. This energy term corresponds to a frequency-dependent “effective temperature” $T_{eff}(f) = E_{eff}(f)/k_B$. At high frequencies ($> 10\text{Hz}$) $T_{eff} \approx 300\text{K}$, whereas at low frequencies $T_{eff} > 300\text{K}$, indicating that the system behaves as if its temperature was increased. Such frequency dependence resembles the results of recent experiments on the nonequilibrium behavior of cytoskeleton-motor systems (21) and the oscillation of hair cells (22), where at high frequency equilibrium thermodynamics dominates whereas at frequencies $< 10\text{Hz}$, the nonequilibrium effects become apparent.

Our finding is of great importance for the theoretical description of RBCs, because our results define a regime in which it is reasonable to apply standard thermodynamics of a single membrane, and one where either out-of-equilibrium phenomena must be taken into account or an extended description of the composite membrane has to be developed. In previous experiments on RBCs such observations were experimentally inaccessible, because their detection requires the knowledge of the full mechanics and access to high-frequency fluctuations, which is generally restricted by the

camera acquisition rate of usually 25Hz. However, it should be noted that the current analysis only shows that a passive membrane model does not explain the behavior at low frequencies, and further experiments are required to prove whether this is because of an active process or requires a more complex description of the composite membrane.

Model. A possible model accounting for the data are sketched in Fig. 4B (17). Note that the presented data reflect the fluctuation of the membrane but does not give direct information about the cytoskeleton, which consists of the floppy spectrin network. This model is based on theoretical suggestions by Gov et al. (12, 23). We attribute the physical origin of the drug dependence to the dissociation of the spectrin-membrane connection. In the context of the 4.1R/spectrin binding, this means that depleting the ATP pool forces the 4.1R protein to be in the unphosphorylated state, which favors the 4.1R/spectrin/actin binding (13, 24). If bound to the membrane, the spectrin cytoskeleton acts like a network of entropic springs, thus imposing a tension that partially compresses the membrane (Fig. 4B) (23). Upon phosphorylation of the 4.1R the spectrin-membrane connection is released and the compressed membrane can relax. The schematics can explain the measured tensions by changes in the spectrin network integrity and variations in the spectrin-membrane interactions, thus leading to modified shear of the spectrin network upon membrane fluctuations. The tension of the spectrin network depends strongly on the network integrity and its association with the membrane. It was already predicted theoretically that at the percolation transition a strong change in tension should be observed (12, 23), which our measurements confirm when modifying the spectrin network by PKC activation or ATP depletion. Increasing the spectrin-membrane connection for ATP-depleted cells leads to an increase in tension, whereas weakening the connection alters the network integrity and hence results in a decrease of tension in PKC-activated cells. As the membrane bending modulus is unaffected by the drugs used, the proposed model predicts that the membrane bending modulus stays constant, as confirmed in our measurements. An additional consequence of the presented model is a nonlinear response to strong deformations caused by a breakdown of the spectrin cytoskeleton at large strains, previously proposed by several authors (25, 26).

The continuous phosphorylation and dephosphorylation of the 4.1R protein is believed to inject mechanical energy in the system. The time scales involved in this binding/unbinding have not yet been determined, but our results indicate that this cycling is slower than 100 ms. In the case of PKC-activation the phosphorylation is favored, however, the cyclic binding/unbinding is not affected, hence energy injection is not perturbed and we measure approximately the same effective energy. The suggested additional dissipative process because of the spectrin-membrane binding might also explain the found increase of effective viscosity in ATP-depleted cells, and its decrease in PKC-activated cells.

Conclusion

In this article we report on a unique, efficient, and fast measurement to detect RBC viscosity, membrane tension, and membrane bending modulus. We confirm theoretical predictions for membrane fluctuations over a wide range of frequencies. The application of ATP-depletion medium and PKC-activation drugs clearly confirms the ATP-dependence of the membrane fluctuations and suggests that the fluctuations might be partially nonthermal in the low frequency domain ($f < 10\text{Hz}$) or that an alternative more complex composite membrane model should be developed for this regime. At high frequencies the system is well described by an equilibrium single membrane theory. Depending on the applied drug, we detect changes in

tension, which we attribute to the coupling of the membrane to the tense spectrin cytoskeleton. The changes in tension might have a role in unfolding the spectrin to expose hidden binding sites in the spectrin which could act as mechanosensors (27). The presented results are also important in the context of other cell organelles, because the spectrin network can be found to be attached to most cell membrane systems, like Golgi membranes, lysosomal membranes, and intracellular vesicles in cerebella neurons, as well as on the plasma membrane (28). Based on previous work by Gov et al. (12), we suggest a model in which the effective energy is provided by a continuous phosphorylation/dephosphorylation of the 4.1R protein, which also alters the spectrin network. The current data does not allow us to decide whether RBC fluctuations are active processes or should be described by a more refined membrane-spectrin interaction. It is also possible that both explanations are required for a full understanding of the RBCs fluctuations.

Materials and Methods

Preparation of RBCs. Human RBCs were freshly prepared before each experiment by finger pricking of a healthy donor. Twenty microliters of blood were diluted in 250 μ L of a PBS solution containing 130 mM NaCl, 20 mM K/Na phosphate buffer, 10 mM glucose, and 1 mg/mL BSA. RBCs were washed twice in the described PBS buffer by centrifugation (2 min, 200 g) and aspiration of the supernatant. Cells were diluted 1:12 in the final experimental buffers. Before the experiment was started, the slight attachment of the cells was checked by RICM microscopy. If not stated otherwise, all materials were purchased at Sigma–Aldrich, France.

Drug Application. We tested RBCs under ATP depletion, PKC activation and LA. ATP depletion was performed by incubating the cells for 3 h at 37 °C in a PBS solution deficient, of Glucose containing 6 mM iodoacetamide and 10 mM inosine, as described previously (11). We found that only 1 h incubation under this condition was not sufficient to significantly reduce the fluctuation amplitudes. Cells were stored in the ATP depletion medium during the experiments. PKC activation was achieved as described previously (13). Briefly, cells were incubate for 30 min at 37 °C with 0.02 μ M calyculin A solved in DMSO

(0.2% final concentration) and subsequently for 90 min at 37 °C with 2 μ M phorbol 12-myristate 13-acetate (PMA). LA was applied at a concentration of 20 μ M LA for 30 min at 37 °C. In the control experiment 0.4% DMSO was applied for 1 h at 37 °C.

Experimental Setup. To measure the fluctuation amplitude of the RBCs edge, we use a technique recently described (14), and summarized in Fig. 1. Laser light from a 1 Watt Ytterbium fiber laser (YLM-1-1064-LP, IPG Photonics, Germany) with a wavelength of 1064 nm is collimated and subsequently intensity controlled by an acousto optical modulator (MT80-A1,5-1064 nm, AA Opto Electronic, France), to reduce the power to 50 μ W at the sample. Up to laser powers of 1 mW, no effect of trapping the RBC was observed (SI Appendix and Fig. S1). A 10 \times telescope increases the diameter of the beam to 14 mm before it is introduced in the beam path of the microscope with a dichroic mirror. The laser is focused in the sample by a 60 \times water objective (UPLSAPO 60XW/IR, NA 1.2). To control the focus and the imaging position the samples are mounted on a 3D piezoelectric stage (Tritor 102 SG, Piezosystem-Jena, Germany). The scattered light is collected by a long distance water-immersion objective (U LUMPL FL 60XW/IR NA 0.9), and projected on a InGaAs QPD (G6849, Hamamatsu, France) by imaging the back focal aperture of the collecting objective on the QPD. The signal was preamplified and finally amplified and anti-alias filtered by a custom made amplification and filtering electronics (Oeffner Electronics, Germany). The signal was digitized at 100 kHz with a 16 bit AD converter card (PCIE-6259, National Instruments, France), and analyzed using LabView (National Instruments) and Matlab (Mathworks, France).

If operated with higher laser power (5 mW), the setup can also be used as an optical tweezer. By trapping 1 μ m beads and recording the PSD of the bead's position we determined the friction coefficient, which is proportional to the medium viscosity (29). For the different media prepared with Dextran 41000 concentrations of 75 mg/mL, 135 mg/mL, and 200 mg/mL we measured the viscosities to be $2.4 \pm 0.1 \times 10^{-3}$ Pa s, $4.4 \pm 0.2 \times 10^{-3}$ Pa s, and $10.9 \pm 0.9 \times 10^{-3}$ Pa s, respectively.

ACKNOWLEDGMENTS. We thank S. Safran, N. Gov, and T. Auth for helpful discussion. This work was supported by the Human Frontier Science Program and a grant of the French Agence Nationale de la Recherche-Physique et Chimie du Vivant. T.B. was supported by a fellowship within the Postdoc Program of the German Academic Exchange Service (DAAD) and by a long-term European Molecular Biology Organization (EMBO) fellowship.

- Bennett V, Baines AJ (2001) Spectrin and ankyrin-based pathways: Metazoan inventions for integrating cells into tissues. *Physiol Rev* 81:1353–1392.
- Brochard F, Lennon JF (1975) Frequency spectrum of the flicker phenomenon in erythrocytes. *Journal de Physique* 36:1035–1047.
- Evans EA (1983) Bending elastic modulus of red blood cell membrane derived from buckling instability in micropipet aspiration tests. *Biophys J* 43:27–30.
- Strey H, Peterson M, Sackmann E (1995) Measurement of erythrocyte membrane elasticity by flicker eigenmode decomposition. *Biophys J* 69:478–488.
- Popescu G, et al. (2006) Optical measurement of cell membrane tension. *Phys Rev Lett* 97:218101.
- Evans J, Gratzler W, Mohandas N, Parker K, Sleep J (2008) Fluctuations of the red blood cell membrane: Relation to mechanical properties and lack of atp dependence. *Biophys J* 94:4134–4144.
- Helfrich W (1973) Elastic properties of lipid bilayers: Theory and possible experiments. *Z Naturforsch C* 28:693–703.
- Discher DE, Mohandas N, Evans EA (1994) Molecular maps of red cell deformation: Hidden elasticity and in situ connectivity. *Science* 266:1032–1035.
- Mohandas N, Evans E (1994) Mechanical properties of the red cell membrane in relation to molecular structure and genetic defects. *Annu Rev Biophys Biomol Struct* 23:787–818.
- Auth T, Safran SA, Gov NS (2007) Fluctuations of coupled fluid and solid membranes with application to red blood cells. *Phys Rev E Stat Nonlin Soft Matter Phys* 76:051910.
- Tuvia S, et al. (1997) Cell membrane fluctuations are regulated by medium macroviscosity: Evidence for a metabolic driving force. *Proc Natl Acad Sci USA* 94:5045–5049.
- Gov NS, Safran SA (2005) Red blood cell membrane fluctuations and shape controlled by atp-induced cytoskeletal defects. *Biophys J* 88:1859–1874.
- Manno S, Takakuwa Y, Mohandas N (2005) Modulation of erythrocyte membrane mechanical function by protein 4.1 phosphorylation. *J Biol Chem* 280:7581–7587.
- Gogler M, Betz T, Kas JA (2007) Simultaneous manipulation and detection of living cell membrane dynamics. *Opt Lett* 32:1893–1895.
- Neuman KC, Block SM (2004) Optical trapping. *Rev Sci Instrum* 75:2787–2809.
- Milner ST, Safran SA (1987) Dynamical fluctuations of droplet microemulsions and vesicles. *Phys Rev A* 36:4371–4379.
- Lee JC, Discher DE (2001) Deformation-enhanced fluctuations in the red cell skeleton with theoretical relations to elasticity, connectivity, and spectrin unfolding. *Biophys J* 81:3178–3192.
- Cokelet GR, Meiselman HJ (1968) Rheological comparison of hemoglobin solutions and erythrocyte suspensions. *Science* 162:275–277.
- Gov N, Zilman AG, Safran S (2004) Hydrodynamics of confined membranes. *Phys Rev E Stat Nonlin Soft Matter Phys* 70:011104.
- Fournier JB, Lacoste D, Raphael E (2004) Fluctuation spectrum of fluid membranes coupled to an elastic meshwork: Jump of the effective surface tension at the mesh size. *Phys Rev Lett* 92:018102.
- Mizuno D, Tardin C, Schmidt CF, Mackintosh FC (2007) Nonequilibrium mechanics of active cytoskeletal networks. *Science* 315:370–373.
- Martin P, Hudspeth AJ, Julicher F (2001) Comparison of a hair bundle's spontaneous oscillations with its response to mechanical stimulation reveals the underlying active process. *Proc Natl Acad Sci USA* 98:14380–14385.
- Gov N, Safran SA (2004) Pinning of fluid membranes by periodic harmonic potentials. *Phys Rev E Stat Nonlin Soft Matter Phys* 69:011101.
- Ohanian V, et al. (1984) Analysis of the ternary interaction of the red cell membrane skeletal proteins spectrin, actin, and 4.1. *Biochemistry* 23:4416–4420.
- Li J, Lykotrafitis G, Dao M, Suresh S (2007) Cytoskeletal dynamics of human erythrocyte. *Proc Natl Acad Sci USA* 104:4937–4942.
- Gov NS (2007) Active elastic network: Cytoskeleton of the red blood cell. *Phys Rev E Stat Nonlin Soft Matter Phys* 75:011921.
- Johnson CP, Tang HY, Carag C, Speicher DW, Discher DE (2007) Forced unfolding of proteins within cells. *Science* 317:663–666.
- Stankewich MC, et al. (1998) A widely expressed beta_{iii} spectrin associated with golgi and cytoplasmic vesicles. *Proc Natl Acad Sci USA* 95:14158–14163.
- Tolic-Norrelykke SF, et al. (2006) Calibration of optical tweezers with positional detection in the back focal plane. *Rev Sci Instrum* 77:103101–103111.

ATP dependent mechanics of red blood cells – Betz *et al.*

Supplementary Information

1 Supplemental Information: Calculations

The power spectral density (PSD) was computed using Matlab as the square of the Fast Fourier Transform (FFT) of the recorded time series y :

$$Y = FFT(y) \quad (1)$$

$$PSD = \frac{Y \times Y^*}{ps}. \quad (2)$$

Here, Y^* denotes the complex conjugate of Y , p is the number of data points in y , and s is the sampling rate of y in Hz. Each value of the PSD corresponds to a frequency f spanning from 0 to the Nyquist frequency $s/2$ with an increment of $\Delta f = s/p$.

To extract the mechanical parameters, the recorded PSDs were fitted by a theoretical expression that is based on the classical Helfrich analysis (1). In the present study we extended previous results from flat membranes (2; 3) to spherical harmonics using expressions derived by Safran and Milner (4).

Plane Membranes The energy of a plane membrane fluctuation is described by a free energy functional:

$$F = \int dA \left[\frac{1}{2} \kappa (\nabla^2 h)^2 + \frac{1}{2} \sigma (\nabla h)^2 \right], \quad (3)$$

where h is the extension of the membrane from its equilibrium position and the integral sums over the whole surface. Using the equipartition theorem the correlation function for the fluctuation reads:

$$\langle h_{\mathbf{q}} h_{\mathbf{q}'} \rangle = \frac{k_B T}{\kappa q^4 + \sigma q^2} (2\pi)^2 \delta(\mathbf{q} + \mathbf{q}'), \quad (4)$$

A fluctuations of wavelength q relaxes at a rate $\omega(q) = (\kappa q^4 + \sigma q^2)/(4\eta q)$ for a impermeable membrane (5; 6), where η is the mean viscosity of the two fluids separated by the membrane. This yield the time dependent correlation function:

$$\langle h_{\mathbf{q}}(t) h_{\mathbf{q}'}(0) \rangle = (2\pi)^2 \delta(\mathbf{q} + \mathbf{q}') \langle h_{\mathbf{q}} h_{\mathbf{q}'} \rangle \exp[-\omega(q)t]. \quad (5)$$

Taking the Fourier transform and integrating over all q modes yields the PSD for a flat membrane:

$$PSD = \int \frac{d^2 \mathbf{q}}{(2\pi)^2} \int_{-\infty}^{\infty} \langle h_{\mathbf{q}}(t) h_{-\mathbf{q}}(0) \rangle \exp(i\omega t) dt \quad (6)$$

$$= \frac{1}{\pi} \int_0^{\infty} q dq \langle h_{\mathbf{q}} h_{-\mathbf{q}} \rangle \frac{\omega(q)}{\omega(q)^2 + \omega^2} \quad (7)$$

$$= \frac{4\eta k_B T}{\pi} \int \frac{dq}{(\kappa q^3 + \sigma q)^2 + (4\eta \omega)^2}. \quad (8)$$

In the limiting cases of high and low frequency we find $PSD \underset{\omega \rightarrow \infty}{=} \frac{k_B T}{12\pi(2\eta^2\kappa)^{1/3}\omega^{5/3}}$ and $PSD \underset{\omega \rightarrow 0}{=} \frac{k_B T}{4\sigma\omega}$. It was suggested in Ref. (3) to include an additional term that reflects an elastic coupling between the membrane and the spectrin network, that extends Eq 3 as:

$$F = \int dA \left[\frac{1}{2}\kappa (\nabla^2 h)^2 + \frac{1}{2}\sigma (\nabla h)^2 + \frac{1}{2}\gamma h^2 \right], \quad (9)$$

where γ is harmonic coupling constant. This additional term changes the PSD expression to (3):

$$PSD = \frac{4\eta k_B T}{\pi} \int_0^{-\infty} \frac{dq}{(\kappa q^3 + \sigma q + \gamma/q)^2 + (4\eta\omega)^2}. \quad (10)$$

Spherical harmonics description The integral [8] is divergent in $\omega \rightarrow 0$. This is due to the fact that a flat membrane has fluctuations divergent in its size. In practice, this is limited by the finite size of the RBC which we take into account using spherical harmonics. This is an extension of previous work (4):

$$r(\Omega) = R(1 + \sum_{l,m} u_{lm} Y_{lm}(\Omega)), \quad (11)$$

where Ω is the solid angle, R is the mean radius of the sphere and Y_{lm} are the spherical harmonics (4). This expression leads to the mean squared amplitude for each fluctuation mode:

$$\langle |u_{lm}|^2 \rangle = \frac{k_B T}{\kappa(l+2)(l-1)l(l+1) + \sigma R^2(l+2)(l-1)}. \quad (12)$$

As before we write the autocorrelation function:

$$\langle u_{lm}(t) u_{l'm'}(0) \rangle = \delta_{l,l'} \delta_{m,m'} \langle |u_{lm}|^2 \rangle \exp(-\omega_l t), \quad (13)$$

where:

$$\omega_l = \frac{\kappa(l+2)(l-1)l(l+1) + \sigma R^2(l+2)(l-1)}{\eta R^3 Z(l)}, \quad (14)$$

with $Z(l) = \frac{(2l+1)(2l^2+2l-1)}{l(l+1)}$. Similar to the case of plane membranes, the Fourier transform of Eq. [13] yields the PSD as:

$$PSD = \int dt \sum_{l=2, m=-l} \langle |u_{lm}|^2 \rangle \exp(-\omega_l t) \exp(i\omega t) \quad (15)$$

$$= \sum_{l=2} \langle |u_{lm}|^2 \rangle \frac{\omega_l}{\omega_l^2 + \omega^2} \frac{2l+1}{2\pi}. \quad (16)$$

This expression was used to fit the measured data in order to get the mechanical parameters κ and σ . The radius R is the average radius of all cells represented in the experimental data set, and the sum was evaluated numerically.

As used for the rescaling in the main text, we separate this expression into the energy source exiting the fluctuations (which we call effective energy $E_{eff}(f)$ in the general case). For the ATP-depleted cells we know that the system is purely passive, and hence we can identify $E_{eff}^{ATP-D} = k_B T$. We write the PSD as product of the energy driving the fluctuations and a term describing the mechanics of the RBC:

$$PSD = E_{eff} \times g(\sigma, \kappa, \eta; f), \quad (17)$$

where:

$$g(\sigma, \kappa, \eta; f) = \sum_{l=2} \frac{1}{\kappa(l+2)(l-1)l(l+1) + \sigma R^2(l+2)(l-1)} \times \frac{\omega_l}{\omega_l^2 + \omega^2} \frac{2l+1}{2\pi}. \quad (18)$$

We rescale the relative amplitude implying the full measured mechanics, thus collapsing all curves onto a master curve. This can be understood by expressing the relative PSDs analytically, where in the passive ATP depleted case, the effective energy is known to be $k_B T$:

$$\frac{PSD_{N,P,L}}{PSD_{ATP-D}} = \frac{E_{eff}(f)}{k_B T} \times \frac{g^{ATP-D}(\sigma, \kappa, \eta; f)}{g^{N,P,L}(\sigma, \kappa, \eta; f)}, \quad (19)$$

where the membrane mechanics are collected in the sum of function g . Hence, the frequency dependent effective energy $E_{eff}(f)$ in units of $k_B T$:

$$\frac{E_{eff}(f)}{k_B T} = \frac{PSD_{N,P,L}}{PSD_{ATP-D}} \times \frac{g^{N,P,L}(\sigma, \kappa, \eta; f)}{g^{ATP-D}(\sigma, \kappa, \eta; f)}. \quad (20)$$

As in the case of the infinite plane membrane, we extend the spherical harmonics expression of the PSD to include the harmonic membrane-spectrin interaction introduced in Ref. (3). This changes $\langle |u_{lm}|^2 \rangle$ to:

$$\langle |u_{lm}|^2 \rangle = \frac{k_B T}{\kappa(l+2)(l-1)l(l+1) + \sigma R^2(l+2)(l-1) + \gamma R^4} \quad (21)$$

and the decay frequency ω_l :

$$\omega_l = \frac{\kappa(l+2)(l-1)l(l+1) + \sigma R^2(l+2)(l-1) + \gamma R^4}{\eta R^3 Z(l)}. \quad (22)$$

2 Supplemental Information: Viscosity correction

Since theory predicts that the effective viscosity should be the average of the internal and external viscosities

$$\eta_{eff} = 1/2(\eta_{RBC} + \eta_{ext}) \quad (23)$$

we varied the external viscosity as presented in the results section. According to theory, η_{eff} should linearly increase with a slope of 1/2 if plotted over the external viscosity η_{ext} . Our data, however, shows a slope of $a = 8.3 \pm 2.3$ (SI-Fig S2) if fitted by a linear function. This experimental observation is thus inconsistent with the theory. From an phenomenological point of view, one may fix this by introducing a prefactor $\alpha = 16.6 \pm 4.6$ which modifies the expression of the effective viscosity to:

$$\eta_{eff} = \alpha/2(\eta_{RBC} + \eta_{ext}). \quad (24)$$

Interestingly, applying this *ad hoc* modification allows to extract a corrected RBC viscosity $\eta_{RBC}^\alpha = 6.4 \pm 1.9$ Pa s, which is consistent with previous measured values (7).

References

- [1] Helfrich, W (1973) Elastic properties of lipid bilayers: theory and possible experiments. *Z Naturforsch C* 28:693–703.

- [2] Helfer, E et al. (2001) Viscoelastic properties of actin-coated membranes. *Phys Rev E Stat Nonlin Soft Matter Phys* 63:021904.
- [3] Gov, N, Zilman, AG, Safran, S (2003) Cytoskeleton confinement and tension of red blood cell membranes. *Phys Rev Lett* 90:228101.
- [4] Milner, ST, Safran, SA (1987) Dynamical fluctuations of droplet microemulsions and vesicles. *Phys Rev A* 36:4371–4379.
- [5] Prost, J, Manneville, JB, Bruinsma, R (1998) Fluctuation-magnification of non-equilibrium membranes near a wall. *The European Physical Journal B - Condensed Matter and Complex Systems* 1:465–480.
- [6] Seifert, U (1994) Dynamics of a bound membrane. *Phys Rev E Stat Phys Plasmas Fluids Relat Interdiscip Topics* 49:3124–3127.
- [7] Cokelet, GR, Meiselman, HJ (1968) Rheological comparison of hemoglobin solutions and erythrocyte suspensions. *Science* 162:275–7.

Supporting Information

Betz et al. 10.1073/pnas.0904614106

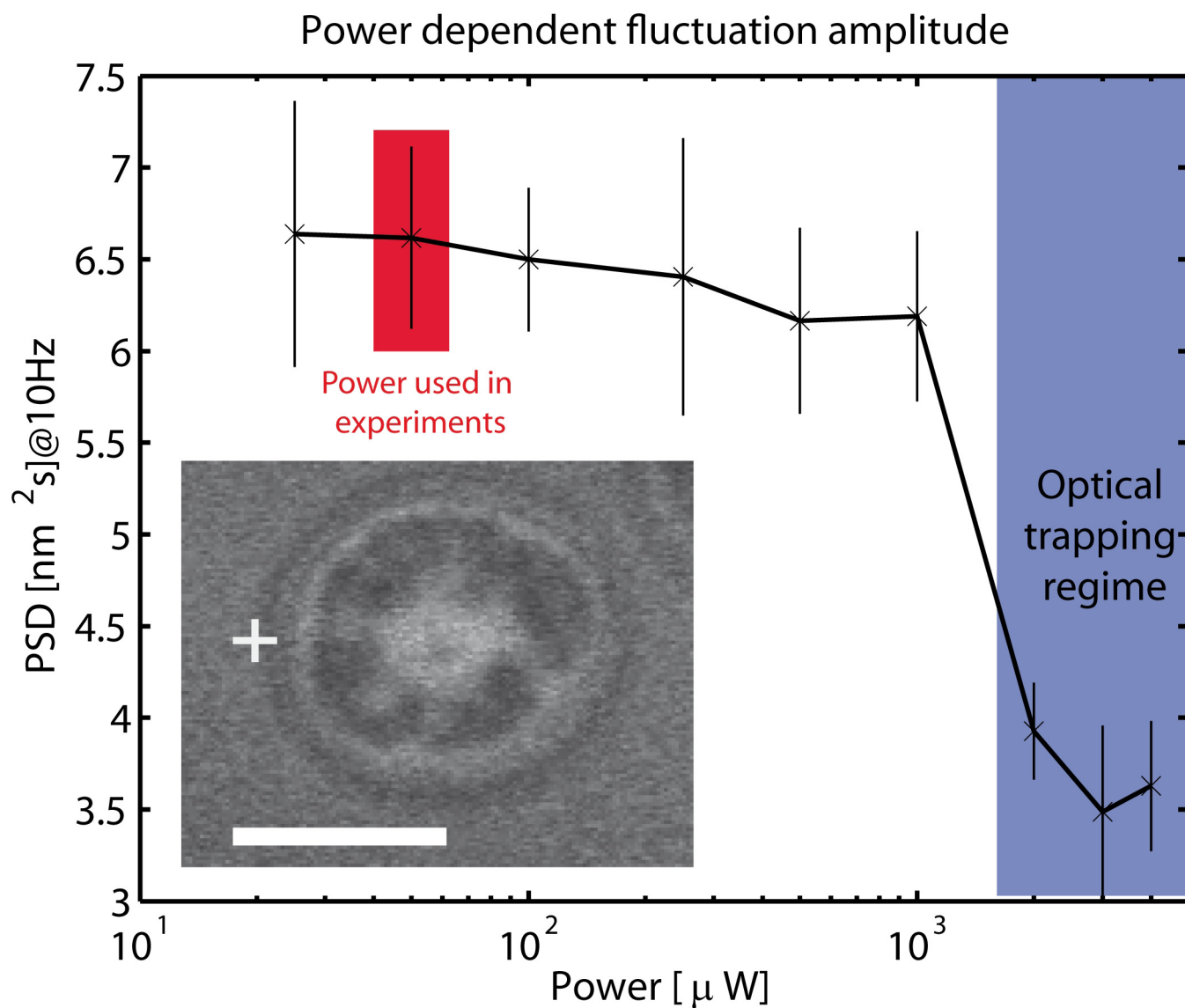


Fig. S1. PSD at 10 Hz as a function of the laser power. Up to 1 mW, the variation in the PSD is within the error, and is hence not significant. At ≈ 1 mW, the pulling force of the laser becomes important, which is reflected in the plot as a strong decrease of the signal, because of the increase of membrane tension whereas pulling of the RBC. (Inset) RICM image of a RBC showing a slight attachment, without a change of the biconcave shape. (Scale bar, $5 \mu\text{m}$.)

PSD and fitted theory for isotonic and swollen RBC

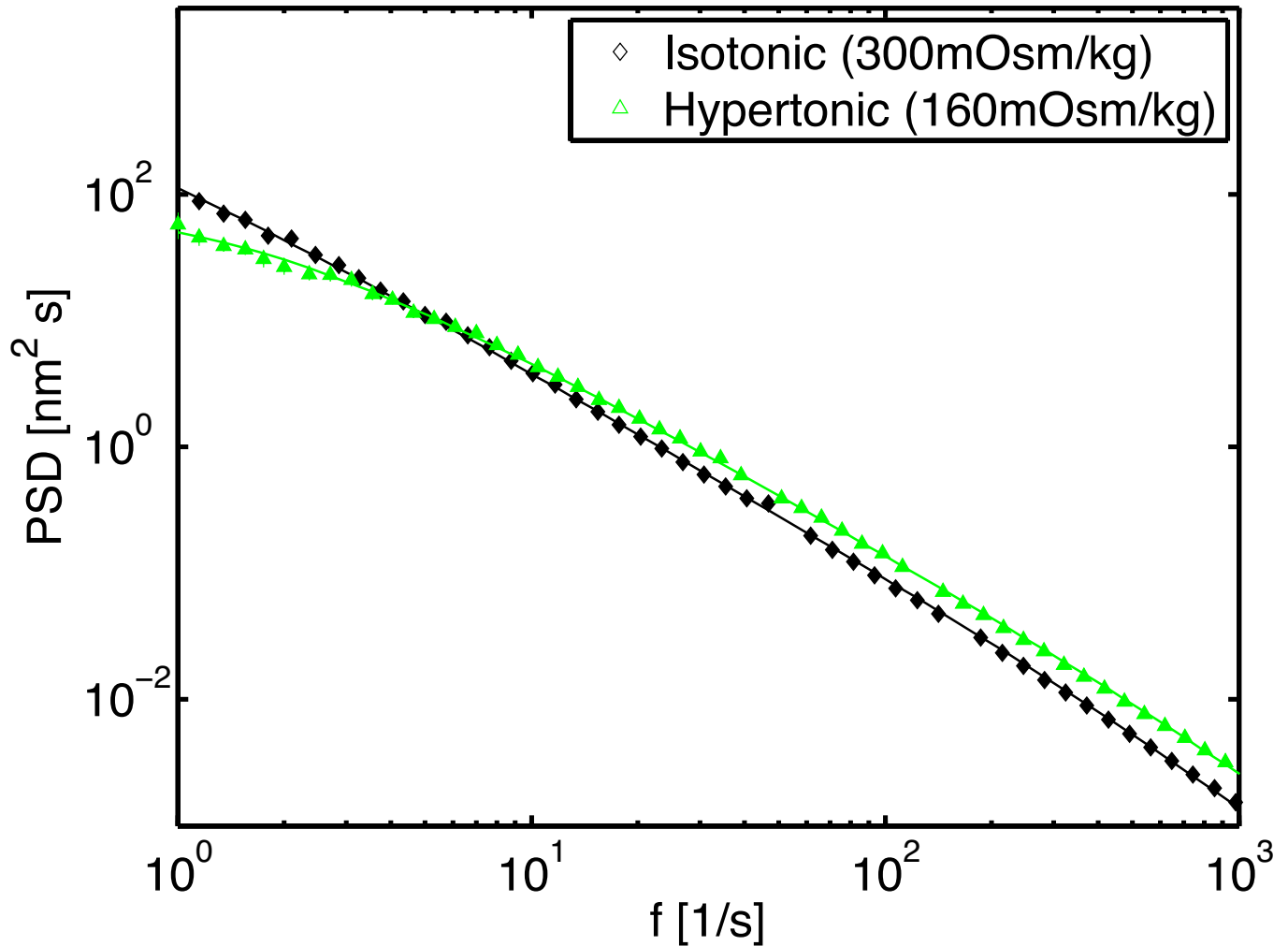


Fig. S2. To confirm the expected change of the PSD in osmotically swollen RBC, we merged the cells in a hypotonic medium with an osmolality of 160 mOsm/kg. In the osmotically swollen cells, the tension increased from normal tension: $\sigma_N = 6.5 \pm 2.1 \times 10^{-7} \text{N/m}$ to swollen tension: $\sigma_s = 24.2 \pm 4.2 \times 10^{-7} \text{N/m}$. The internal viscosity was decreased from $\eta_N = 81 \pm 3.7 \times 10^{-3} \text{Pa s}$ to $\eta_s = 42 \pm 1.7 \times 10^{-3} \text{Pa s}$ consistent with the influx of water. The bending rigidity was almost unchanged between the normal cells $\kappa_N = 2.8 \pm 0.3 \times 10^{-19} \text{J}$ and the swollen cells $\kappa_s = 2.4 \pm 0.3 \times 10^{-19} \text{J}$. These results further support our analysis method, as they yield the expected results of osmotic swelling.

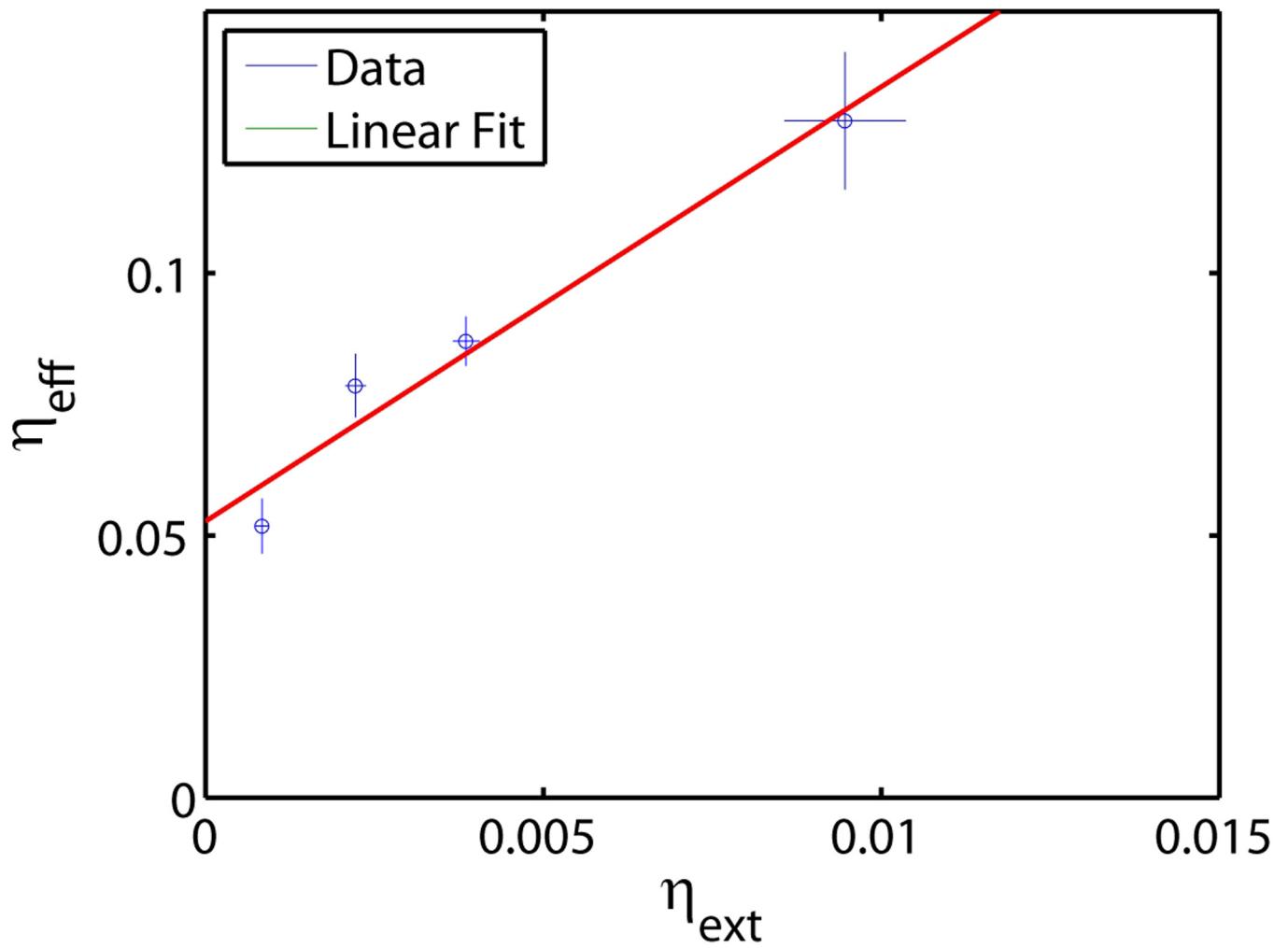


Fig. S3. Measured effective viscosity η_{eff} plotted as a function of the external viscosity η_{ext} . This phenomenological plot can be fitted by a simple linear function $\eta_{\text{eff}} = a \times \eta_{\text{ext}} + b$, yielding fit parameters of $a = 8.3 \pm 2.3$ and $b = 53 \pm 11 \times 10^{-3} \text{Pa s}$.

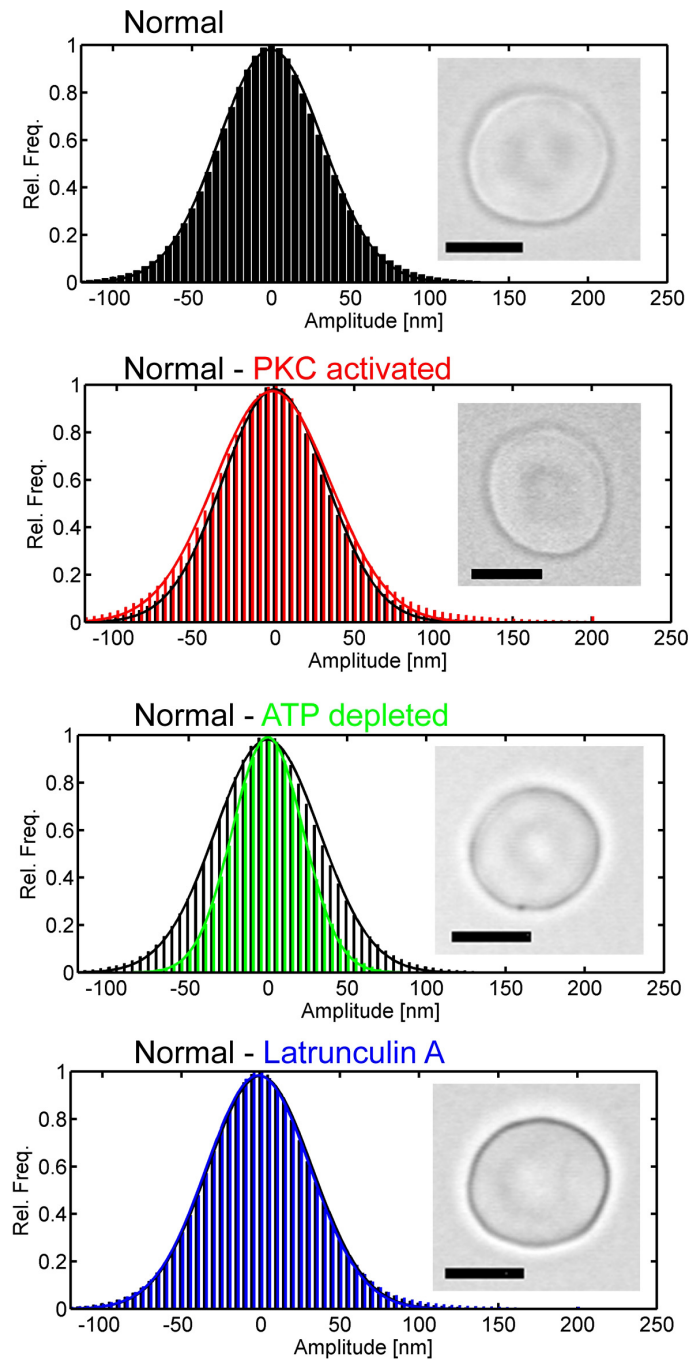


Fig. S4. Fluctuation amplitude histograms of normal (black), ATP-depleted (green), PKC-activated (red) and latrunculin A (blue)-treated cells. Straight lines present Gaussian fits of the respective histogram. The data shows that ATP-depleted cells have a significantly smaller fluctuation amplitude, whereas the fluctuations of PKC and LA-treated cells are similar.

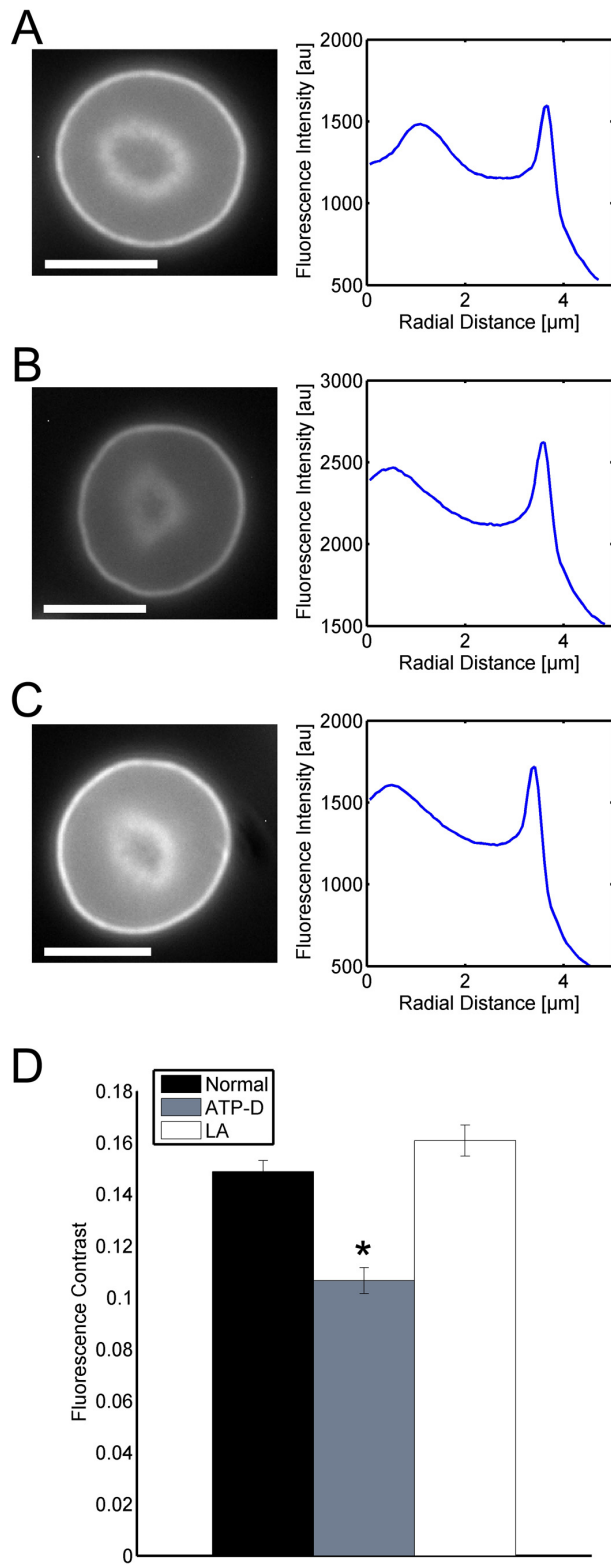


Fig. S6. (A) Fluorescence image of an F-actin stained normal RBCs. The radial intensity line as presented in the plot is averaged >100 center edge intensities. The contrast is determined by $c = \frac{M - m}{M + m}$, where M and m are the peak intensity at the rim and the minimal intensity in the cell, respectively. (B) Same as A, but for an ATP-depleted cell. (C) Same as A, but for a LA-treated cell. (D) Resulting contrast values for each 20 cells, giving a significantly reduced contrast in the ATP-depleted cells.

Fluctuation decrease over time

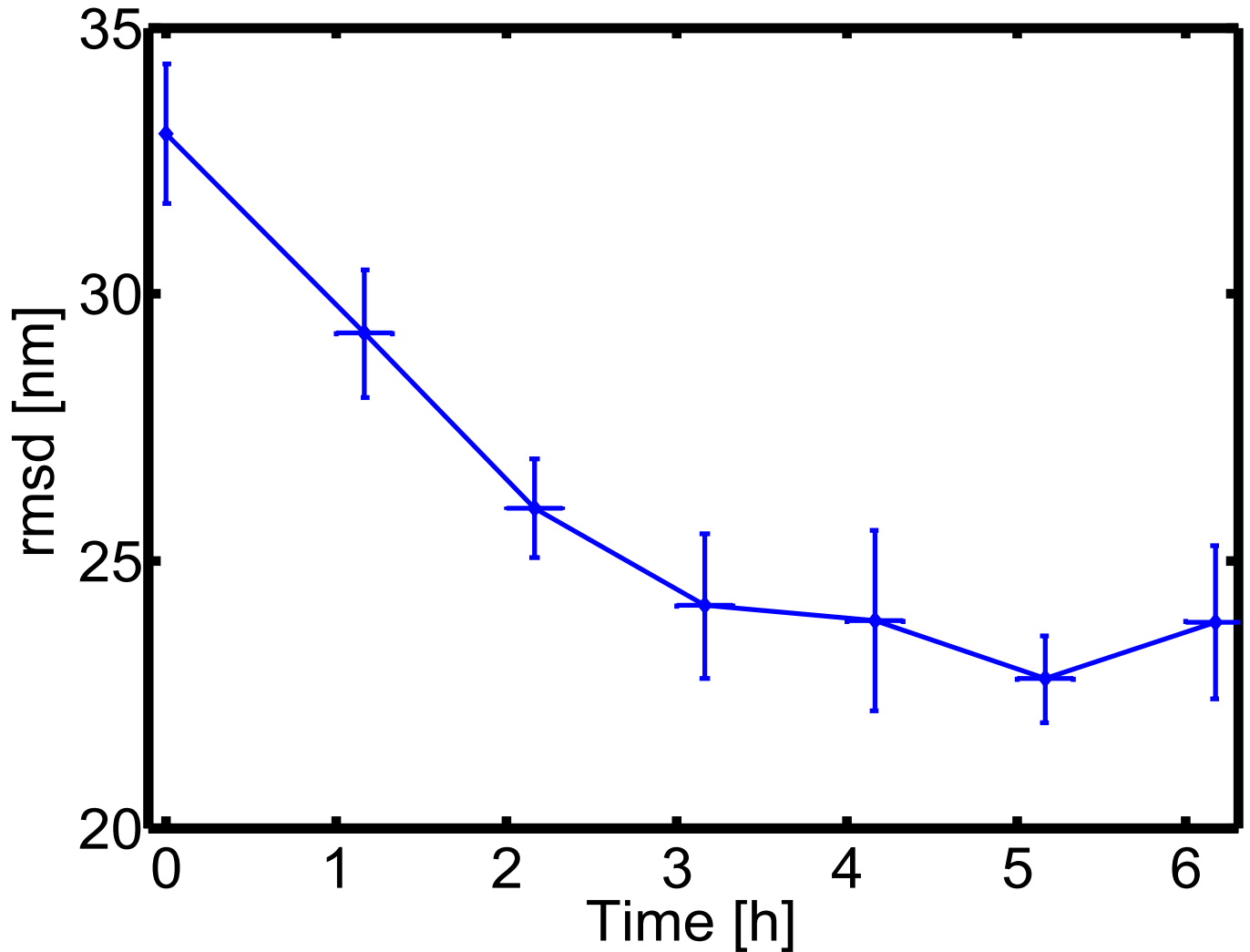


Fig. S7. Kinetic study of ATP-depletion effect. Rmsd as a function of the time during which the ATP-depletion buffer is applied. Each datapoint represents ≈ 50 experiments on usually 10 different cells. It should be noted that after 1 h the cells start to slowly deviate from the circular geometry, and after 6 h, most cells have turned into echinocytes. For the data acquisition, round and slightly deformed cells were mixed, but echinocytes were excluded. We record already after 1 h a significant reduction in fluctuation amplitude measured by the rmsd. After 3 h this reduction levels out, and after 6 h the measurement becomes impossible because almost all cells have deformed into echinocytes.

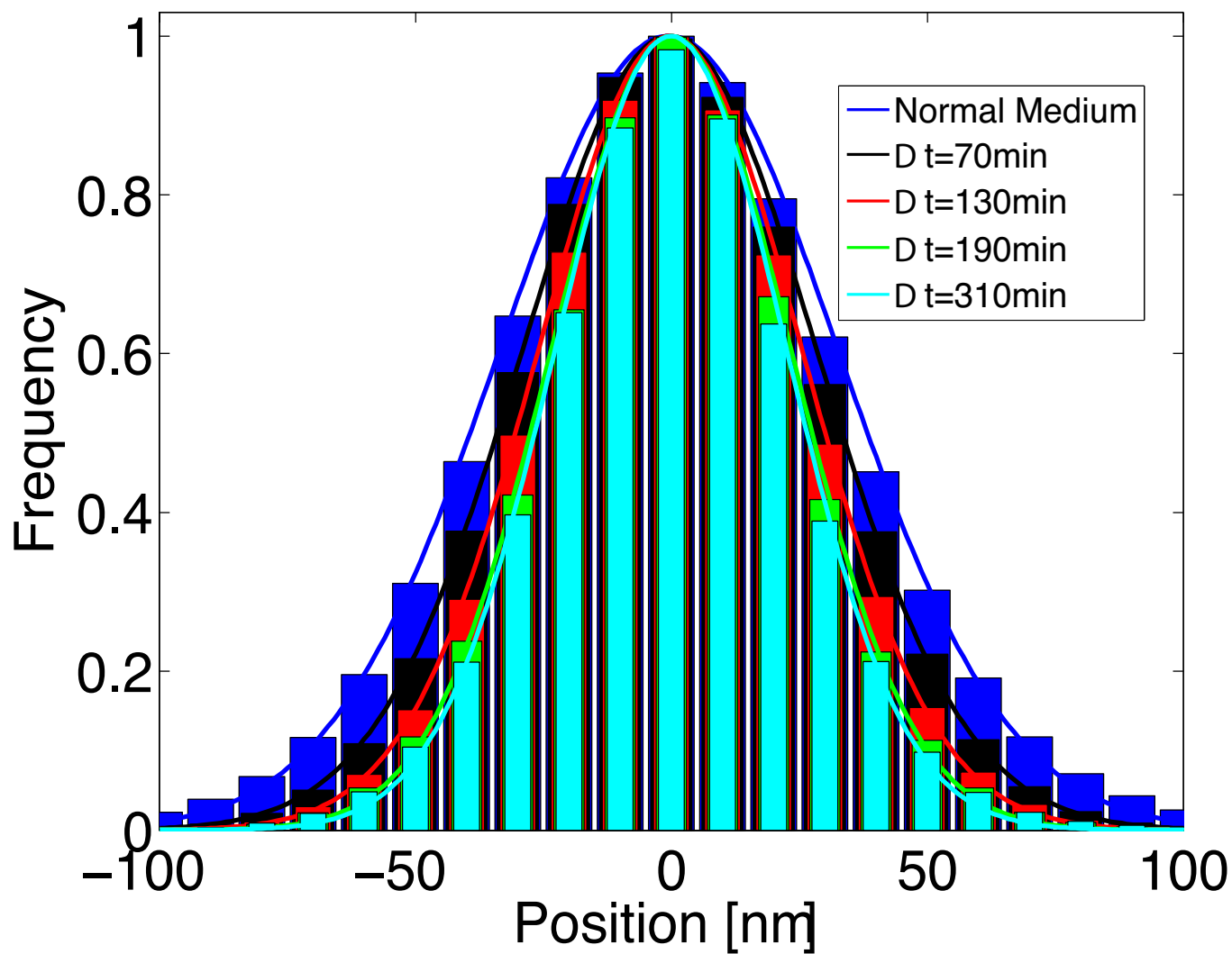


Fig. S8. Histogram of the edge fluctuation for the each ATP-depletion buffer application time. The figure overlays five time points, showing a steady decrease in fluctuation amplitude over time. All histograms represent the overlay of the ≈ 50 experiment at the given time of incubation (see legend). The histograms are well fitted by a Gaussian distribution.

Table S1. Collection of mechanical parameters of RBCs under various conditions, including the gamma term in the fit function

| | Normal | ATP-depl. | PKC | LA |
|-----------------------------------|-----------------|----------------|----------------|----------------|
| $rmsd_{ex}$ [nm] | 33.0 ± 1.3 | 22.3 ± 0.6 | 36.7 ± 2.8 | 32.8 ± 2.2 |
| κ^{stat} [10^{-19} J] | 2.8 ± 0.3 | 6.1 ± 0.6 | 2.3 ± 0.2 | 2.8 ± 0.3 |
| κ^{dyn} [10^{-19} J] | 2.9 ± 0.3 | 3.9 ± 0.3 | 2.6 ± 0.2 | 2.7 ± 0.2 |
| σ [10^{-7} N/m] | 6.5 ± 2.1 | 19 ± 1 | 2.7 ± 1.1 | 4.7 ± 1.0 |
| η_{eff} [10^{-3} Pa s] | 81 ± 3.7 | 118 ± 11.7 | 57 ± 2.4 | 55 ± 4.0 |
| γ [10^{-8} Jm $^{-4}$] | 0.06 ± 0.04 | 4.9 ± 2 | 5.2 ± 2.0 | 6.6 ± 5.9 |

Other Supporting Information Files

[SI Appendix \(PDF\)](#)